Electronic reading of a mechanical gas meter based on a dual magnetic sensing

Edgar Ripoll-Vercellone, Manel Gasulla and Ferran Reverter

Department of Electronic Engineering, Universitat Politècnica de Catalunya - BarcelonaTech, Castelldefels (Barcelona), Spain

E-mail: ferran.reverter@upc.edu

Received xxxxxx
Accepted for publication xxxxxx
Published xxxxxx

Abstract

This article proposes a measurement system controlled by a microcontroller unit (MCU) for the electronic reading of a mechanical gas meter. The measurement relies on a dual magnetic sensing: 1) a low-cost low-power primary sensing based on reed switches connected to digital inputs of the MCU, and 2) a secondary sensing based on Hall-effect sensors connected to analogue inputs of the MCU. In addition, both sensing strategies have an active and a passive element to achieve an output insensitive to external interfering magnets. A prototype has been implemented and characterized under different test conditions to confirm its reliability.

Keywords: Embedded system, gas meter, Hall-effect sensor, magnetic sensor, microcontroller, reed switch

1. Introduction

The application of the information and communications technology to the power grid has led to the concept of smart grid [1], with the corresponding benefits in the energy production and distribution. In such a context, smart electronic meters, mainly for the electricity sector [2], have been designed and deployed at the end-consumers' home.

For the gas sector, most meters (see figure 1a) are still mechanical, and the reading of the mechanical index is carried out by either the end user or a worker of the gas company every one-two months. In order to avoid such a manual reading and obtain a smarter meter, these mechanical gas meters can be complemented/upgraded with electronic measurement and communication systems. Actually, many gas meters have a rotating magnet inside (from now on, *meter magnet*, as shown in figure 1b) that allow an electronic reading; this is the case of the diaphragm gas meters from Itron and Elster–Honeywell, which are two of the main manufacturers. This meter magnet can be detected, for instance, through a low-cost reed switch connected to a microcontroller unit (MCU) [3,4]. Its main limitation, however, is that the reading can be easily altered by an external interfering magnet. Other more expensive solutions have also been proposed in the literature for gas meters, such as optical encoders [5] and vision camera [6].

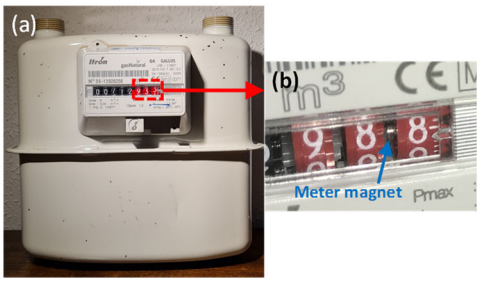

Figure 1. (a) Mechanical gas meter. (b) Meter magnet behind the least-significant drum of the mechanical index.

The use of additional sensors to better extract the information of interest is quite common in electronic measurement systems [7,8]. This is also applied in utility meters, for example: 1) magnetic sensors (such as Hall-effect sensors) are employed in electricity meters to detect the tampering caused by external magnets [9,10], and 2) magnetic

sensors (such as reed switches) are proposed for detecting the theft or detachment of gas meters [11]. However, the detection of the meter magnet of a gas meter in the presence of an external interfering magnetic field is still a challenge. This is tackled herein by incorporating additional sensors to the basic reed switch-based configuration [3,4].

2. Electronic circuit

Figure 2 shows the proposed MCU-based circuit with a dual magnetic sensing: 1) a primary (default) sensing that relies on reed switches [3,4], and 2) a secondary sensing carried out by Hall-effect sensors. Both sensing strategies have an active and a passive element, as in strain gauges to compensate for interfering effects [12]. The active elements are placed as close as possible to the position of the meter magnet to be very sensitive to it. The passive elements are placed at the minimum distance from the corresponding active element that provides a "zero" sensitivity to the meter magnet. The shorter the distance, the more similar the effects of the interfering magnet on both sensors. Overall, the circuit has four sensors:
a) *Primary Active Sensor* (PAS), which detects the meter magnet in normal conditions, i.e. without interfering effects.
b) *Primary Passive Sensor* (PPS), which detects the interfering effects and, hence, activates the secondary sensing.
c) *Secondary Active Sensor* (SAS), which monitors the meter magnet in unusual conditions, i.e. with interfering effects.
d) *Secondary Passive Sensor* (SPS), which monitors the interfering effects in unusual conditions.

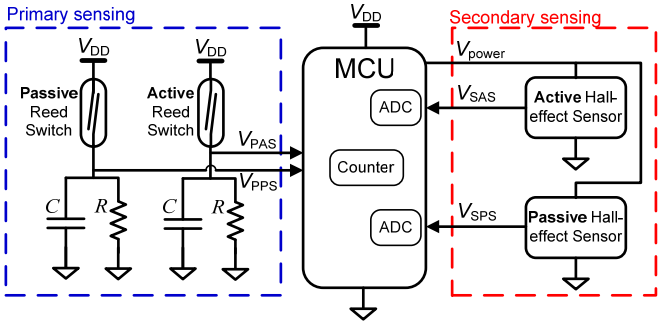

Figure 2. Schematic of the proposed circuit.

The PAS and PPS are connected, via an RC de-bouncing circuit, to digital inputs of the MCU with external interrupt capability, whereas the SAS and SPS are connected to analogue inputs with an embedded analogue-to-digital converter (ADC). Except when the meter magnet is aligned to the SAS, the output voltage of the SAS and SPS (V_{SAS} and V_{SPS}, respectively) should be ideally the same. However, this is not practically true due to the tolerance of the sensors, and the fact that the interfering magnet will not equally affect both of them. The MCU also includes a digital counter that increases by 1 every time that the meter magnet passes in front of the active sensors, thus counting the gas consumption with a resolution of 0.01 m^3.

With the aim of reducing the current consumption of the design, SAS and SPS are only supplied when required. To do so, a digital output (V_{power} in figure 2) of the MCU provides a digital "1" to the supply voltage pin of these sensors only when the secondary sensing needs to be active. By default, V_{power} provides a digital "0" and, hence, these sensors do not consume energy.

Most of the commercial reed switches and Hall-effect sensors available in the market operate correctly in the industrial temperature range (i.e. from –40 to +85ºC), which is clearly wider than the expected operating range of the gas meter even if this is placed outdoors. In addition, integrated Hall-effect sensors usually include a temperature-compensation circuitry so that the analogue output is almost insensitive to temperature changes. The typical value of the temperature coefficient of the magnetic sensitivity is around 0.02%/ºC [13]. Accordingly, an extreme change of the ambient temperature of 50ºC would cause a change of 1% in the sensitivity and, hence, in the amplitude of the pulse generated by the presence of the meter magnet. This change is completely negligible for the application considered herein.

3. Firmware

A flowchart of the algorithm executed by the MCU is shown in figure 3. First, an "Initialization & configuration" stage sets the different peripherals of the MCU. In addition, the secondary sensing is temporally activated with the aim of measuring V_{SPS} at rest conditions; its value is stored in the variable $V_{SPS,0}$. Next, the flowchart has five main stages:
- *Stage A*, which corresponds to the normal operating conditions without the presence of an interfering magnet. The system relies on the primary sensing and the counter is increased by 1 at each rising edge of V_{PAS} provided that V_{PPS} is "0". If V_{PPS} is "1", the secondary sensing is activated.
- *Stage B*, which is intended to obtain the difference $V_{SAS} - V_{SPS}$ once V_{SPS} is stable, i.e. when the interfering magnet has a fixed position. Such a difference, which is stored in the variable ΔV_{ref}, is expected to be different than zero since the interfering magnet will not equally affect SAS and SPS.
- *Stage C*, which checks the presence and/or movement of the interfering magnet. First, a double check on V_{PPS} and V_{SPS} confirms either the presence or absence of the interfering magnet. Second, any change of position of the interfering magnet is detected by comparing V_{SPS} with that obtained in stage B (stored in the variable $V_{SPS,ref}$). And third, the factor $\Delta V = V_{SAS} - V_{SPS} - \Delta V_{ref}$ is computed. We expect $\Delta V = 0$ under no effects of the meter magnet, and $\Delta V > 0$ under its effects. If $\Delta V < 0$, it means that ΔV_{ref} was computed in stage B with the meter magnet effects and, hence, it has to be recalculated.
- *Stage D*, which detects the effects of the meter magnet on SAS. When the meter magnet is aligned to SAS, V_{SAS} increases and $\Delta V > 0$. If ΔV is higher than a certain threshold, then the counter is increased by 1. In addition, an internal

variable (M) is set to "1", which indicates that the meter magnet has been already detected by the secondary sensing.
- *Stage E*, which checks when the SAS is not anymore under the effects of the meter magnet. This is inferred by comparing ΔV with zero. When this is the case, M is set again to "0" to be able to detect the next magnet-SAS alignment.

To have a more stable algorithm, the values of V_{SAS} and V_{SPS} correspond to the average of 10 measurements. In addition, the comparison between analogue voltages in Fig. 3 takes into account a certain level of uncertainty around the expected value. To optimize the energy consumption in unusual operating conditions, the MCU is by default in sleep mode, executes the algorithm every 50 ms, and enables the Hall-effect sensors (via the V_{power} signal) during 1 ms.

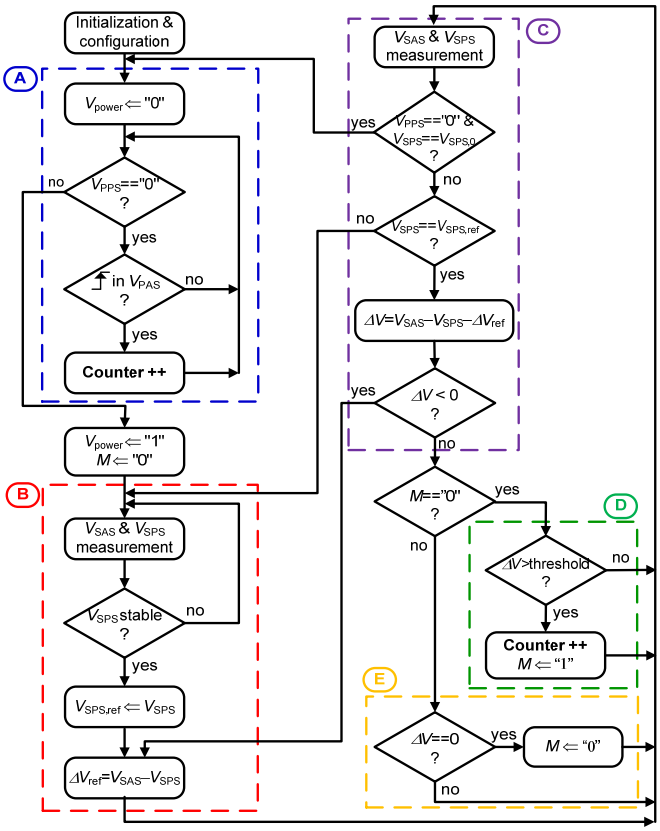

Figure 3. Flowchart of the algorithm executed by the MCU.

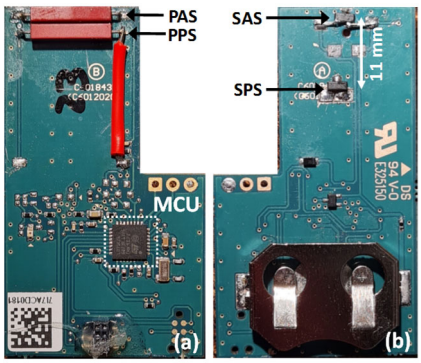

Figure 4. PCB developed: (a) top layer, and (b) bottom layer.

4. Experimental results

A prototype of the circuit in figure 2 was developed in a printed circuit board (PCB), as shown in figure 4. The MCU (STM32L071KZU from STMicroelectronics) ran on a 32-kHz crystal oscillator. This MCU has an embedded 12-bit ADC with a resolution (or a least-significant bit, LSB) of 0.8 mV when the supply voltage (V_{DD}) is 3.3 V. The Hall-effect sensor (AH49ENTR-G1 from Diodes Incorporated, with a nominal sensitivity of 16 mV/mT) was selected to have a wide magnetic field range (±0.1 T) and, hence, avoid its saturation due to the interfering magnet. The reed switch was the CT10-2540-G1 from Coto Technology, and $R = 560\ k\Omega$ and $C = 5.6$ nF. Table 1 summarises the main costs to develop the proposed design.

Table 1. Cost of the main components to develop the design shown in figure 4 assuming a high-volume production.

Component	Cost (€)
PCB	1.00
MCU	1.40
32-kHz crystal	0.26
Reed switches (×2)	0.69
Hall-effect sensors (×2)	0.63
Battery	0.16
Battery holder	0.17
TOTAL	**4.32**

Figure 5. Placement of the PCB shown in figure 4 into the gas meter: (a) without the protecting box, (b) with the protecting box.

The PCB had the appropriate physical dimensions to be placed into the gas meter, as shown in figure 5. The primary sensing was placed at the top layer, whereas the secondary sensing at the bottom, as shown in figure 4. The active sensors (PAS and SAS) were positioned at the border of the PCB to be as close as possible to the meter magnet; when the meter magnet was aligned, the distance to the active sensors was around 10 mm. On the other hand, the passive sensors (PPS and SPS) were placed at 2 and 11 mm, respectively, from the

corresponding active element. Using such distances, the PPS was insensitive to the meter magnet, whereas the SPS was at least ten times less sensitive to the meter magnet than the SAS.

To easily characterize the prototype, the gas injected to the meter inlet was air through an electric air pump. An external disc magnet, with a diameter of 4.8 cm, was employed to generate the interfering magnetic field. This magnet was completely attached to the front, top, and lateral of the mechanical index of the meter; although being attached, the minimum distance to the sensors was around 12 mm. In the worst testing scenario, this magnet caused (at the sensors position) an interfering magnetic field of 50 mT. On the other hand, the meter magnet generated (at the active sensors position) a magnetic field of 0.6 mT, which is 80 times lower than the previous one.

Figure 6 shows the experimental waveforms acquired by a digital oscilloscope under no effects of an interfering magnet. In such conditions, the PPS provided a digital "0", whereas the PAS generated a rising edge, which increased the value of the counter by 1, when the meter magnet became aligned to it. The signal provided by the PAS was activated for a time interval of 900 ms, which would correspond to a gas consumption of about 133 l/min. Of course, the lower the gas consumption, the longer the activation time.

The most critical interfering scenario was when the interfering magnet was attached to the front of the mechanical index of the meter. Figure 7 shows the experimental waveforms of V_{SAS} and V_{SPS} when the interfering magnet was placed at three different front positions; the signals provided by PAS and PPS are not represented there but they were a digital "1". According to figure 7, when the meter magnet was aligned to SAS, V_{SAS} increased by 10 mV regardless of the position of the interfering magnet, whereas V_{SPS} was almost constant. An increase of 10 mV corresponds to a change of 12 LSB at the ADC output. From figure 7, we can also see that the baseline of V_{SAS} and V_{SPS} (and, hence, the difference $V_{SAS} - V_{SPS}$) depended on the position of the interfering magnet, but this was dynamically corrected by the algorithm proposed in figure 3.

In normal operating conditions and when the reed switches were open, the circuit in figure 2 had a current consumption of 5 µA, which was mainly due to the sleep mode of the MCU. However, when the secondary sensing was active, the average current consumption increased up to 86 µA. Therefore, the robustness in front of interfering magnets is at the expense of a higher current consumption.

After proving the feasibility of the proposed measurement subsystem, this could be complemented with: 1) a communication subsystem using a Low-Power Wide-Area Network (LPWAN) technology, and 2) an energy harvester, such as a low-area photovoltaic panel, especially for those gas meters located outdoors. The energy consumption of the communication subsystem is expected to be higher than that of the measurement subsystem, but the sensor node could still be autonomous thanks to the energy harvester.

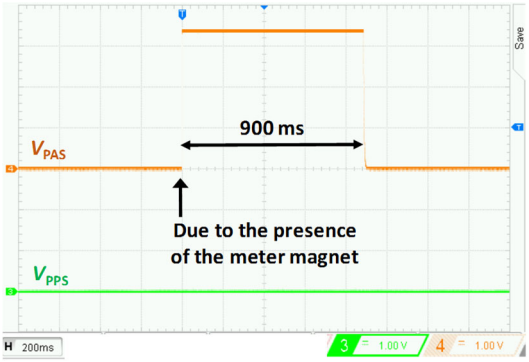

Figure 6. Waveforms acquired from the PAS and PPS when the meter magnet was detected under no interfering magnet effects.

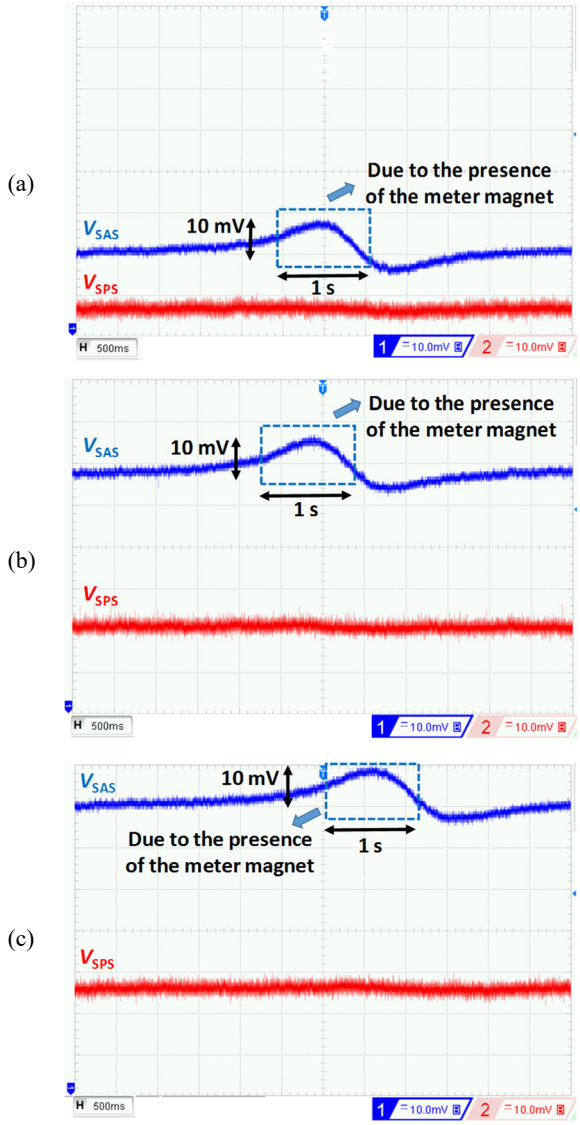

Figure 7. Waveforms acquired from the SAS and SPS when the meter magnet was detected and the interfering magnet was at three different positions at the front of the meter. The ground level of channels 1 and 2 was moved down (not visible in the screenshots) at different positions to better appreciate the effects of the meter magnet on both signals, but it was at the same position for the three cases represented.

5. Conclusions

In the context of smart meters for smarts grids, this article has proposed an MCU-based circuit for upgrading mechanical gas meters into electronic ones. The suggested circuit together with a dynamically-adjusted algorithm are able to detect the meter magnet under the effects of an interfering magnet and, in addition, the interfering magnet itself does not cause an erroneous increase of the digital counter. Consequently, the proposed sensor system has been proven reliable in the event of static magnetic fields generated by interfering magnets.

Acknowledgements

This work was supported by the Secretariat of University and Research of the Ministry of Business and Knowledge of the Government of Catalonia, and by the Spanish Ministry of Economy and Competitiveness and the European Regional Development Fund under project TEC2016-76991-P.

References

[1] Duarte D P, Nogueira R N and Bilro L B 2019 Semi-supervised Gaussian and t-distribution hybrid mixture model for water leak detection *Meas. Sci. Technol.* **30** 125109

[2] Rinaldi S, Ferrari P, Flammini A, Sisinni E and Vezzoli A 2019 Uncertainty analysis in time distribution mechanisms for OMS smart meters: the last-mile time synchronization issue *IEEE Trans. Instrum. Meas.* **68** (3) 693–703

[3] Rorato O, Bertoldo S, Lucianaz C, Allegretti M and Notarpietro R 2013 An ad-hoc low cost wireless sensor network for smart gas metering *Wirel. Sens. Netw.* **5** (3) 61–66

[4] Kot T 2015 Flow measurement with reed switches and BLE *App. Rep. TIDUB33*, Texas Instruments

[5] Tewolde M, Longtin J P, Das S R and Sharma S 2013 Determining appliance energy usage with a high-resolution metering system for residential natural gas meters *Appl. Energy* **108** 363–372

[6] He Z, He Y, Yang Y and Gao M 2017 A low-cost direct reading system for gas meter based on machine vision *Proc. 12th IEEE Conf. Industrial Electronics and Applications* 1189–1194

[7] Qiu S, Huang Y, He X, Sun Z, Liu P and Liu C 2015 A dual-mode proximity sensor with integrated capacitive and temperature sensing units *Meas. Sci. Technol*. **26** (10) 105101

[8] Praveen Kumar T, Saimurugan M, Hari Haran R B, Siddharth S and Ramachandran K I 2019 A multi-sensor information fusion for fault diagnosis of a gearbox utilizing discrete wavelet features *Meas. Sci. Technol.* **30** 85101

[9] Keith Seal B and Martin B 2007 Magnetic field sensing for tamper identification *US Patent* 2007/0229256 A1

[10] Ramirez A D 2015 Magnetic tampering detection in a utility meter *US Patent* 2015/0002134 A1

[11] Yukihiro O 2012 Gas meter theft sensing device *Patent* WO2012157264A1

[12] Pallàs-Areny R and Webster J G 2001 *Sensors and signal conditioning* (New York: John Wiley & Sons)

[13] Honeywell Inc. Sensing and control *Hall effect sensing and application* https://sensing.honeywell.com/hallbook.pdf